Materials Research Proceedings 41 (2024) 1551-1558 https://doi.org/10.21741/9781644903131-172

# Numerical analysis of flanging using tailored rubber pad forming on AA7075-O sheets

BORREGO-PUCHE Marcos[1,a], PALOMO-VÁZQUEZ David[1,b], MORALES-PALMA Domingo[1,c*], MARTÍNEZ-DONAIRE Andres Jesus[1,d], ROSA-SAINZ Ana[1,e], CENTENO Gabriel[1,f] and VALLELLANO Carpoforo[1,g]

[1]Dpt. Mechanical and Manufacturing Engineering, University of Sevilla, Spain

[a]mborrego@us.es, [b]dpalomo1@us.es, [c]dmpalma@us.es, [d]ajmd@us.es, [e]arosa@us.es, [f]gaceba@us.es, [g]carpofor@us.es

**Keywords:** Sheet Metal Forming, Rubber Pad Forming, Flanging, Flangeability

**Abstract.** The flanging of metal sheets is extensively used in the automotive and aeronautical industries to provide rigidity or support for subsequent assembly. Flanging by rubber pad forming is one of the most common processes for small and medium batch production. Flanges with non-linear bending lines are exposed to severe conditions that significantly hinder our comprehension of the geometrical, material, and process factors associated with flange formability (i.e., flangeability). This work presents a numerical study of the flanging process by a tailored rubber pad of hollow AA7075-O parts with continuous concave and convex flanges. The flangeability limits, the geometric capabilities of the forming process, and the deformation mechanisms of stretched and shrunk flanges as well as in the transition zone between them are analysed.

## Introduction

The flanging process is widely established in the automotive and aeronautical industries to provide stiffness or support for further assembly in sheet metal parts. This consists of bending, usually at 90º, the perimeter of the part along a given line. Regarding the curvature of the bending line, three elemental types of flanges can be distinguished in: straight, concave, or convex flange. In concave flange, also referred to as stretch flange, the material is subjected to a combination of bending and stretching. The most likely mode of failure is localized necking and/or ductile fracture. And in convex flange, also named shrink flange, the material withstands bending and compression, being the appearance of wrinkling the expected mode of failure. Different combinations of these elemental flanges are also common in industrial practice.

Conventional flanging used in medium- or small-batch production, as usual in the aeronautical industry, is mainly performed by rubber pad forming and hydroforming. Despite their technical importance, the conventional flanging processes are subjected to strong restrictions that greatly limit the process. Thus, the interest of scientists and technicians in understanding the geometric, material and process parameters that limit the formability of the flange (i.e., flangeability) in industrial practice is not surprising [1-4].

This work presents a numerical study of flanging hollow 7075-O aluminium alloy sheet parts with continuous concave and convex flanges by rubber pad forming. The objective is to evaluate the forming capabilities of the process to manufacture combined stretch and shrink flanges. The preliminary numerical results show severe difficulties to form the flanges of the proposed specimen as well as excessive forces. The use of tailored rubber pads is required to better distribute pressure, improve flange deformation, and reduce overall forces. Flangeability limits, geometric capabilities of the forming process and deformation mechanisms of stretch and shrink flanges, as well as in the transition zone between them, are analysed.

## Methodology

The proposed specimen of analysis is based on the work of Zhang et al. [5], consisting of a clover-shaped hole (see Fig. 1(a)) that allows forming 3 stretch flanges and 3 shrink flanges in a single sample. The flange height $h_0$ and radii $R_{stretch}$ and $R_{shrink}$ of the specimens were selected from typical values used in aeronautical ribs.

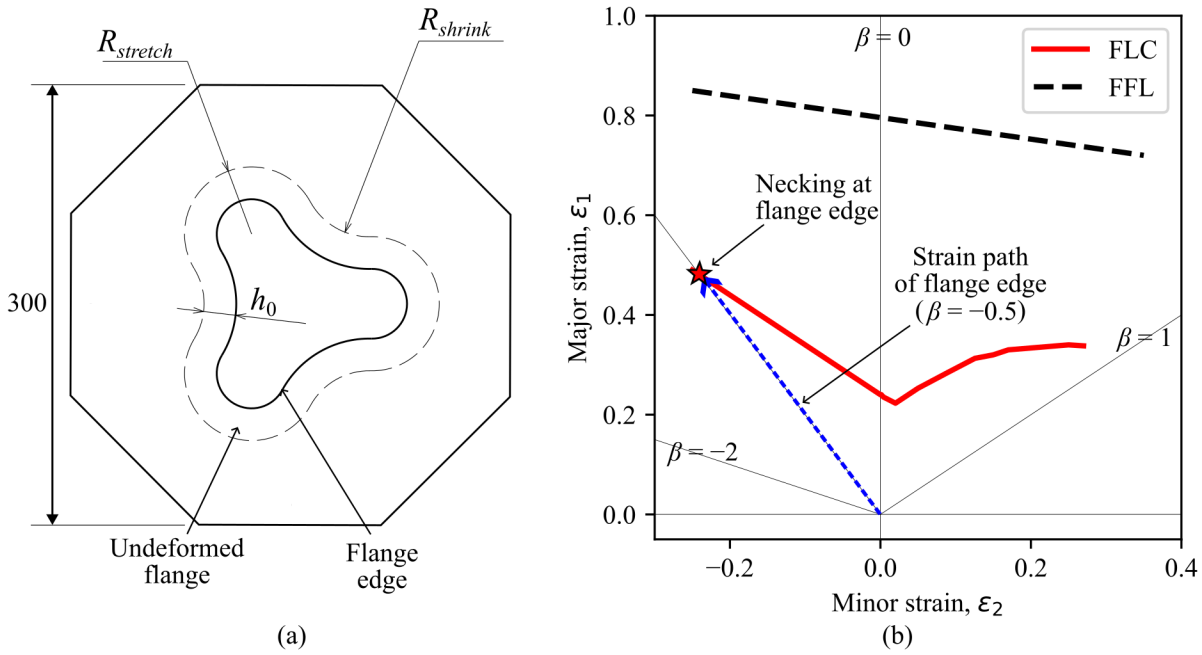


*Fig. 1: (a) Schema of the parametrized sheet blank; (b) FLD (Forming Limit Diagram) for AA7075-O sheets showing predicted localized necking at the flange edge (FLC is the Forming Limit Curve for localized necking and FFL is the Fracture Forming Limit).*

Different values of $R_{stretch}$ (25, 50 and 75 mm) and $R_{shrink}$ (0, 25, 50, 100 mm and ∞) have been tested by simulations to obtain flanged parts with different combinations of the characteristic failure modes of conventional sheet metal forming: localized necking prior to fracture, and wrinkling. This work presents the modelling and simulation of a selected specimen that allows to produce both types of failure simultaneously.

As a reference value for the flange width $h_0$, it has been considered the one that would produce localized necking just at the end of the flanging operation. Knowing that necking will occur at the edge of the hole, the reference value for $h_0$ can be estimated from the major principal strain at the flange edge by

$$\varepsilon_1 = \ln\left( R_{stretch} / (R_{stretch} - h_0) \right) \quad (1)$$

and assuming uniaxial tension conditions.

Fig. 1(b) shows the FLD (Forming Limit Diagram) for the material under study: 1.6 mm thick 7075-O aluminium alloy sheets [6-7]. As represented in the FLD, necking will occur when the strain path at the edge reaches the FLC (Forming Limit Curve for localized necking), i.e. $\varepsilon_1 = 0.5$ approximately (see Fig. 1(b)) [6]. Substituting in Eq. (1) for a radius $R_{stretch} = 50$ mm, the reference value is $h_0^* = 19.7$ mm. However, to ensure that failure occurs, a slightly larger flange width should be chosen. Thus, in this work, a specimen with the following dimensions has been considered: $R_{stretch} = R_{shrink} = 50$ mm and $h_0 = 21$ mm.

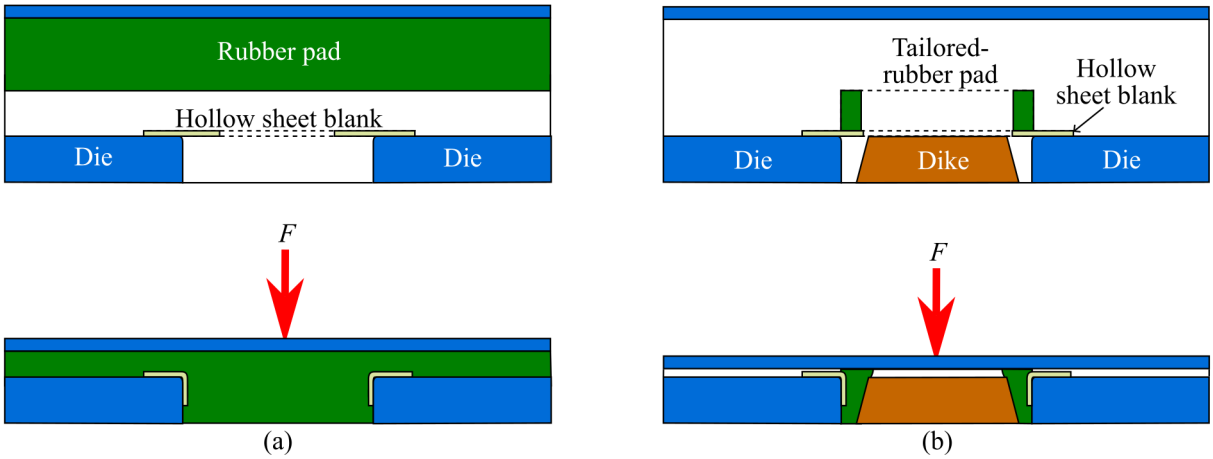


*Fig. 2: Schema of rubber pad forming: (a) conventional process; and (b) tailored rubber pad forming.*

Specimens are to be tested by rubber pad forming. Fig. 2(a) shows a schema of this process. In general, a high-capacity press is required to form the sheet metal part from the rubber pad (or set of pads). The alternative process proposed in this work is shown schematically in Fig. 2(b). It basically consists of replacing the large rubber pads with a single rubber pad of tailored geometry to exert pressure only on the area of the part to be formed, avoiding redundant work and thus reducing the forming force. In order to keep the pressure of the rubber tool on the sheet metal part, a rigid dike must be carefully designed and integrated, as represented in Fig. 2(b).

**Numerical Simulations**

Numerical simulations have been carried out to evaluate conventional and proposed tailored rubber pad forming, using the commercial finite element (FE) code Abaqus/Explicit. Fig. 3 shows schematically the design procedure of the FE models. Fig. 3(a,c) present the setup for the conventional rubber pad forming and tailored rubber pad forming, respectively. To reduce the computational cost of the simulations, the models have been reduced to a 60º section by two symmetry planes relative to the deformation of the sheet, see Fig. 3(b,d). All part modelling has been developed with CATIA V5. Fig. 3(e) presents the parts meshing with Abaqus of one of the FE models.

The rubber tooling is modelled as a deformable part of 3D elements. The sheet blank is modelled as a deformable part of 2D-shell elements with five integration points through the thickness. All the degrees of freedom of the nodes on the outer edge of the blank are fixed to simplify the clamping of the blank. The die and the dike are modelled as discrete rigid parts. An analytical rigid horizontal plane is used to press on the rubber pad. This plane is not shown in Fig. 3 for clarity.

The rubber material is a polyurethane rubber with Shore hardness 90 A. The Mooney-Rivlin theory ($C_1$ = 2.824, $C_2$ = 0.706) is used to model the hyperelastic behaviour of rubber [8]. The sheet material is 7075-O aluminium alloy sheet of 1.6 mm thickness. Its mechanical properties are $E$ = 70 GPa, $\nu$ = 0.33 and $YS$ = 109.5 MPa. The von Mises yield criterion and a law $\sigma = 314\ \varepsilon^{0.13}$ are used to describe the plasticity behaviour and hardening of the metal sheet, respectively.

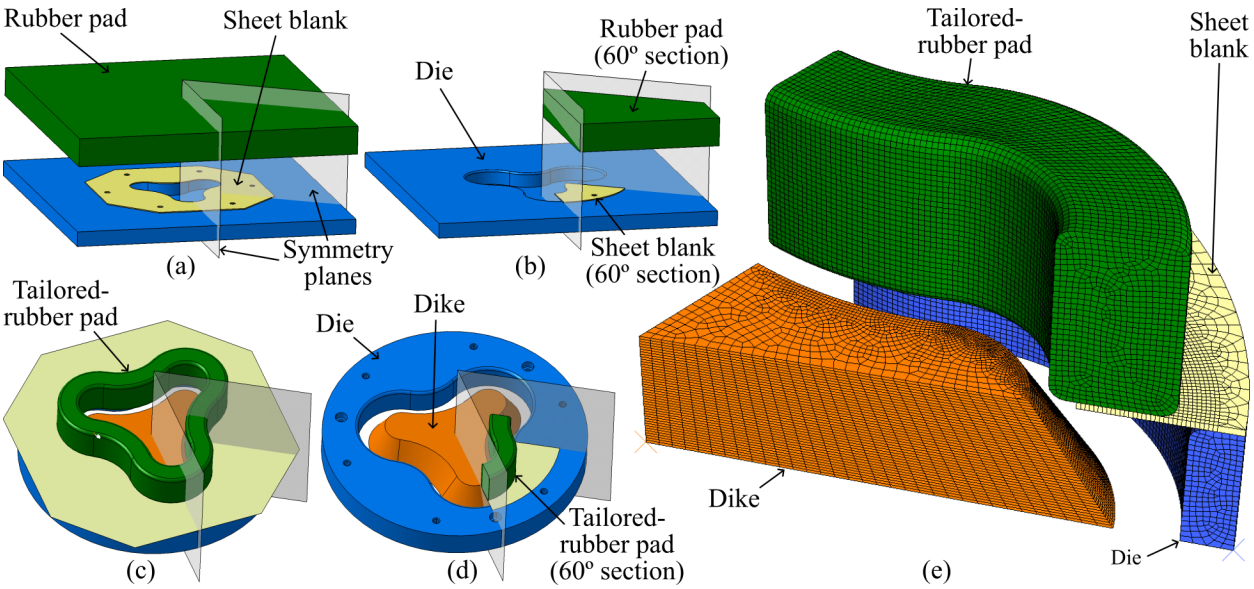


*Fig. 3: Schema of the numerical models: (a) conventional rubber pad forming; (b) simplified model by using symmetry planes; (c) tailored rubber pad forming; (d) corresponding simplified model; and (d) meshing of parts.*

The rubber pad and flange area of the sheet blank are meshed with elements of size 0.8 mm approximately. For the rest, elements between 2 and 4 times larger are used to reduce the computational cost (see Fig. 3(e)). A surface-to-surface contact algorithm with the finite slip formulation is used. A Coulomb friction coefficient of 0.3 is assumed in all part contacts.

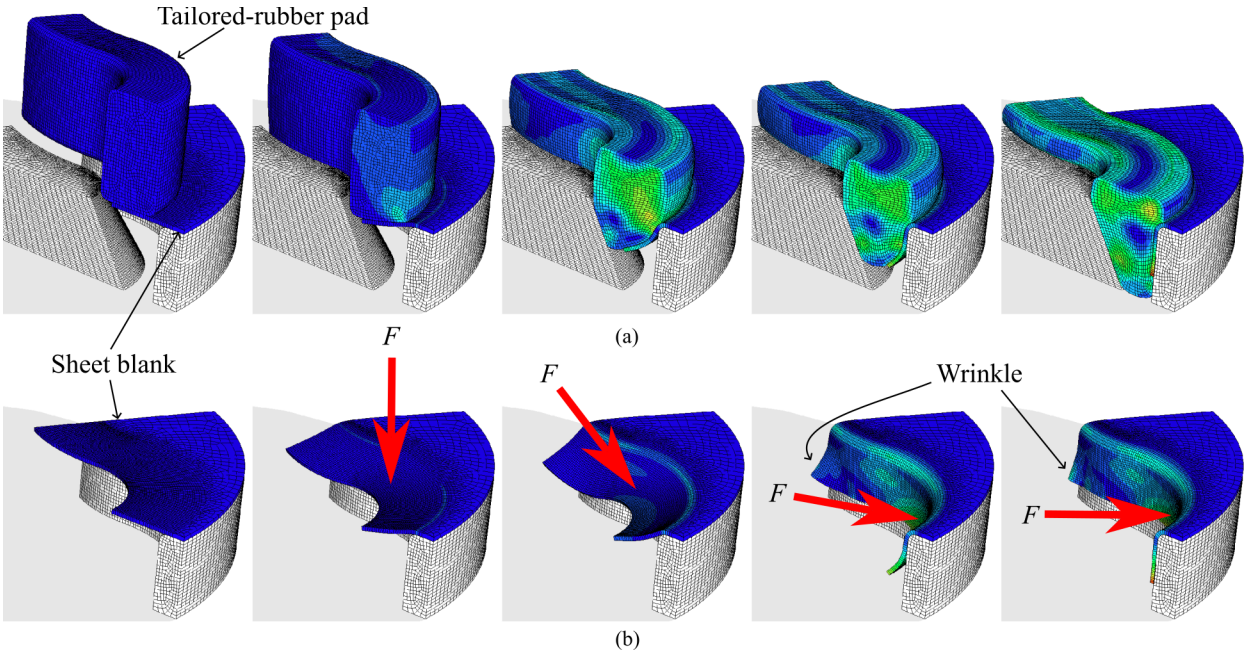


*Fig. 4: Simulation of the deformation of: (a) the tailored rubber pad; and (b) the flanged sheet metal specimen.*

Simulations of conventional rubber pad forming predicted a required press force greater than 3 MN for the specimen under study. Instead, for the tailored rubber pad forming simulations, forces in the range of 300-550 kN were obtained, i.e. 10 times less than the conventional process.

Fig. 4 shows the deformation of tailored rubber pad and sheet metal in the simulation of tailored rubber pad forming. As can be seen in Fig. 4(a), the rubber is compressed between the dike and the die and pushes the sheet against the die to finish the complete folding. Fig. 1(b) shows the formation of a small wrinkle in the compressed flange region at the end of the forming process.

Fig. 5 presents the major ($\varepsilon_1$) and minor ($\varepsilon_2$) in-plane principal plastic strain distributions in outer and inner sheet surfaces. Red elements in Fig. 5(a) indicate that the more stretched material is the edge in the stretched flange region. A maximum value of $\varepsilon_1 = 0.547$ was found at the edge, on the inner surface of the flange, a few centimetres from the symmetry plane in the stretched flange region (see Fig. 5(a) bottom). This is a very accurate prediction since, as described below, experimental tests show that localized necking and subsequent tearing of the flange occurs very close to this point.

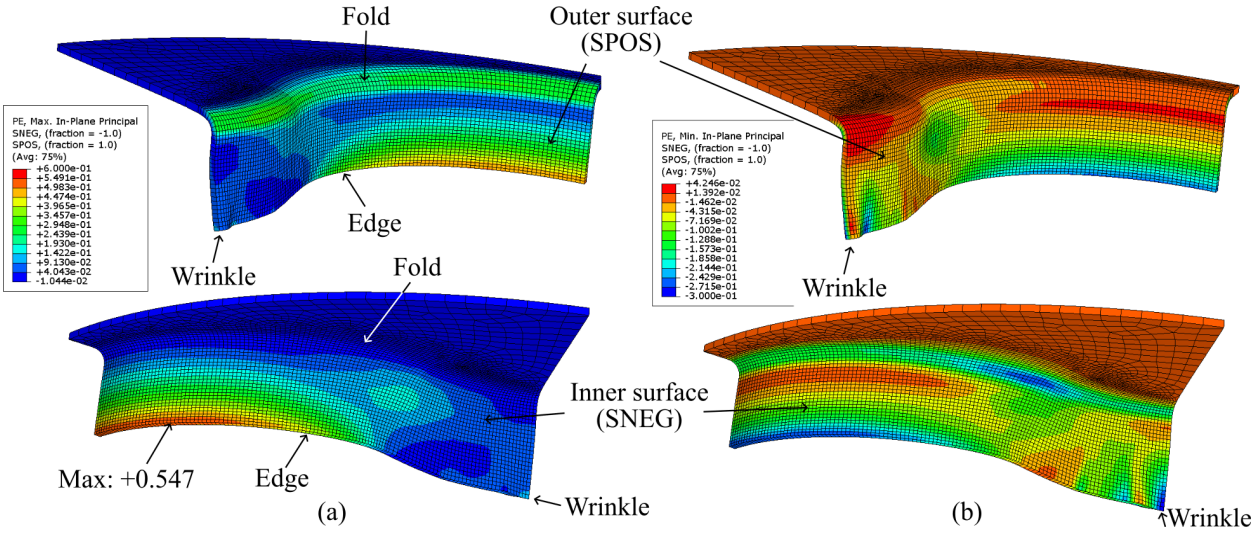


*Fig. 5: (a) Major and (b) minor in-plane principal plastic strains on both surfaces of the metal sheet.*

As can be seen from the strain contours in Fig. 5, there are substantial differences in strains between the two sheet surfaces in some areas, especially along the fold and the wrinkle. This indicates a significant strain gradient through the sheet thickness. Such strain gradients can be better analysed in the FLD of Fig. 6. This Fig. depicts the strain distribution along the flange on both sheet surfaces in 3 different regions: (a) in the symmetry plane of the compressed flange region, (b) in the transition between compressed and stretched flange regions, and (c) in the symmetry plane of the stretched flange region. As can be seen, the strain gradient in the fold remains similar in all 3 regions. Regarding the edge, there is a noticeable strain gradient through the sheet thickness only in the compressed region of the flange due to the wrinkle (see Fig. 6(a)). Necking in the stretched flange region is also clearly predicted in Fig. 6(c), given that the strain at the edge exceeds the FLC on both sides of the sheet. It should be noted that although the strain at the outer surface of the fold exceeds the FLC in some regions (see Fig. 6(a,c)), this does not indicate necking due to the strain gradient through the sheet thickness [6].

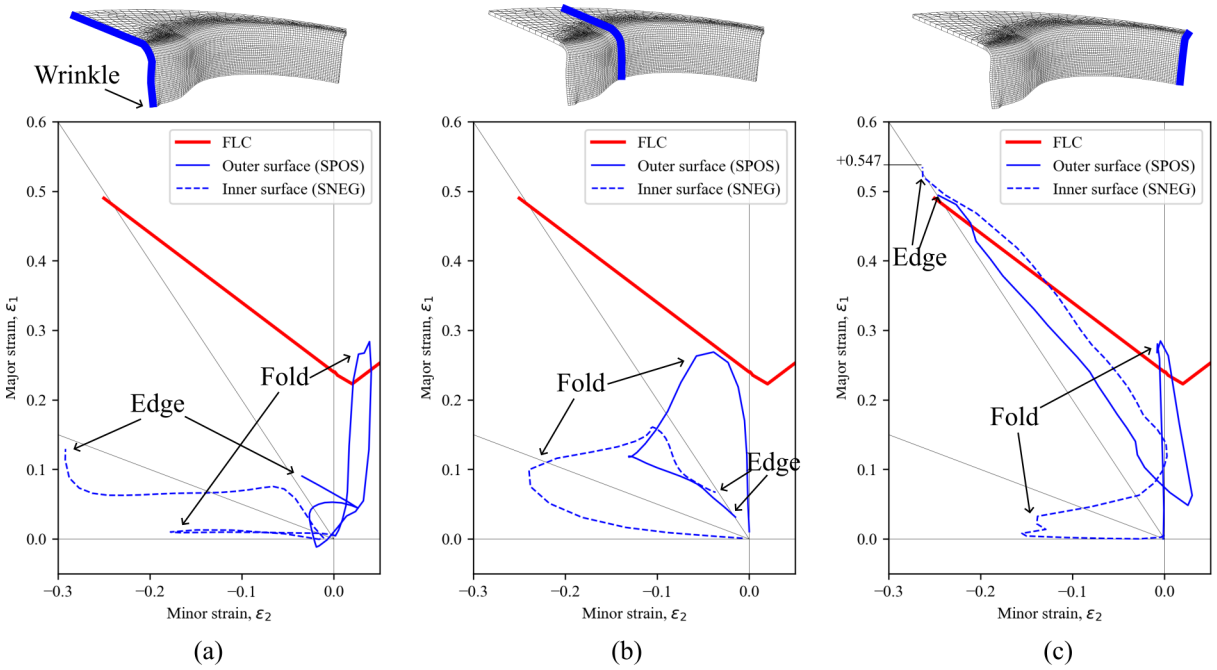


*Fig. 6: Strain distributions along the flange: (a) compressed region; (b) transition; (c) stretched region.*

**Experimental Validation**

Tailored rubber pad forming experimental tests were performed to validate the numerical analysis. The experiments were carried out using the setup depicted in Fig. 7(a,b). Die, dike, tailored rubber pad and blank metal sheets were designed and manufactured to meet the experimental plan and to be interchangeable. The rubber pad was lubricated with Vaseline. The testing machine has a capacity of 600 kN and a stroke speed of 1 mm/s was used. The forming load and travel were monitored during the tests.

The tailored rubber pad (Fig. 7(b)) was produced by moulding in a silicone mould for polyurethane. To fabricate the silicone mould, a PLA (PolyLactic Acid) pattern was manufactured on an FFF (Fused Filament Fabrication) 3D printer. Using the same procedure, cylindrical specimens were also fabricated to validate by compression testing that the hardness of the polyurethane rubber is around Shore 90 A.

The metal blanks were machined on an EMCO UMILL 630 CNC machining centre. The hole edges were subsequently ground with fine grit sandpaper to eliminate any burrs. Fig. 7(c,d) depicted a tested specimen viewed from both surfaces. As can be seen, the two types of failure predicted in the numerical simulation occurred very accurately. On the one hand, a small wrinkle was produced right in the middle of each shrink flange (i.e. in the plane of symmetry used in the numerical model). On the other hand, a localized necking occurred at the edge at a location very close to that predicted by the numerical simulation, which caused the crack propagation shown in Fig. 7(c,d).

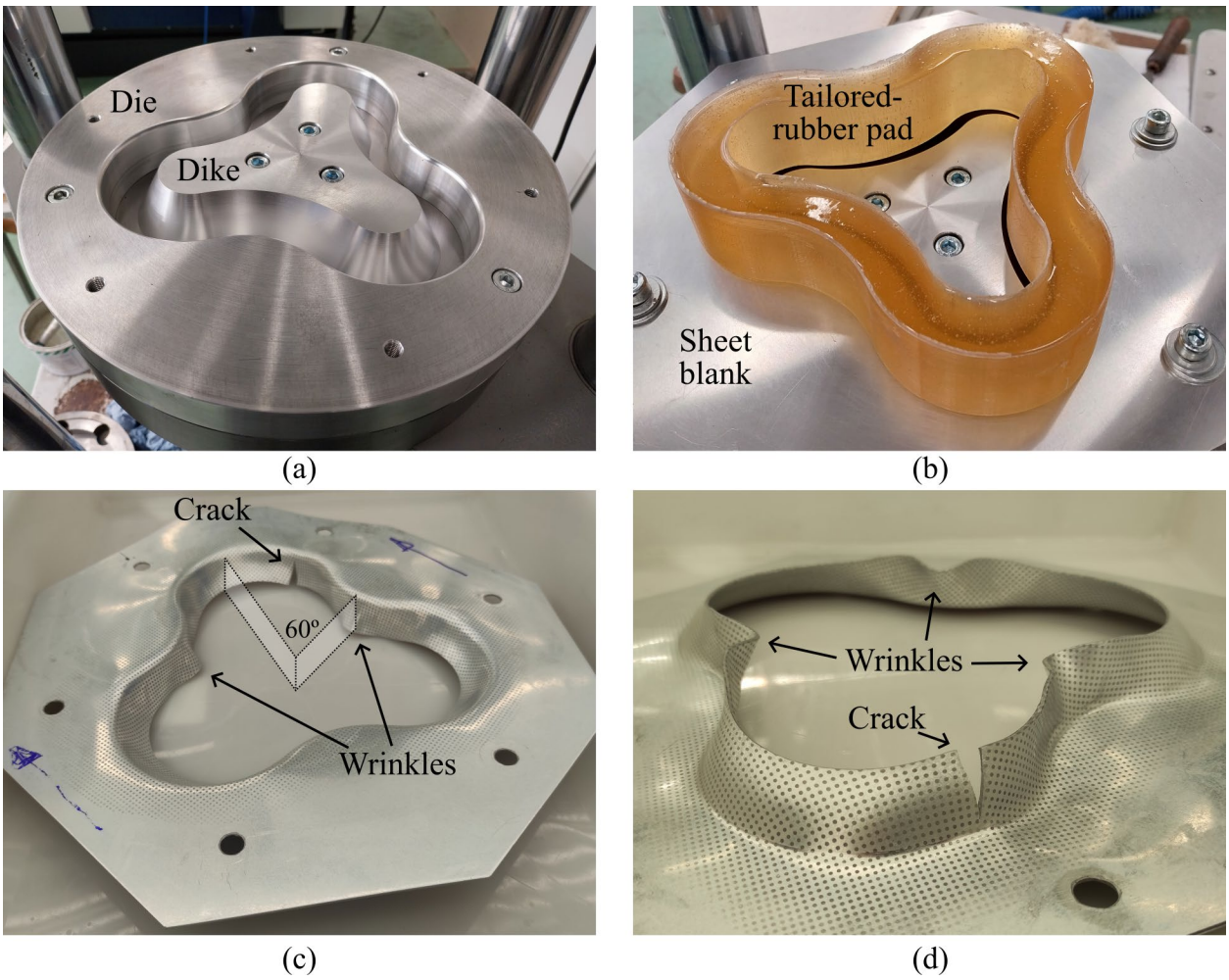


*Fig. 7: Experimental setup showing (a) die, dike, (b) tailored rubber pad, sheet blank, and (c-d) the manufactured part.*

**Conclusions and Further Work**

Flanging by tailored rubber pads of hollow AA7075-O sheet parts with continuous stretch and shrink flanges has been designed and numerically analysed using FE simulations. The following conclusions can be drawn from this study:

- The FLD is a valuable tool for the design of sheet metal parts. In this work the FLC has been used to accurately estimate the flange size that would produce a failure by necking and/or fracture in the flange edge.
- The appearance of wrinkles can be predicted by FE simulations using different values of radius in shrink flanges ($R_{shrink}$). This provides a practical alternative to theoretical/analytical methods of predicting such instabilities.
- The results obtained allow establishing a robust specimen design methodology to address a flanging test campaign to elucidate safe conformability windows in terms of variables used in the literature such as $h/R$ and $R/t$.
- Tailored rubber pads are easy to manufacture, e.g. by liquid moulding, and provide a cost-effective alternative in the equipment for flanging complex parts. In this sense, simulation results facilitate the design of these flexible elements as well as of the specimens, dies and tools.

As mentioned above, the next step is to carry out a campaign of numerical and experimental flanging tests to elucidate the safe conformability windows of AA7075-O sheets and other aeronautical materials by tailored rubber forming. A comparative study using an incremental forming process (SPIF, Single-Point Incremental Forming) to perform the flange operations is also planned.

**Acknowledgements**
The authors acknowledge the funding provided by Grant PID2021-125934OB-I00 financed by MCIN/AEI/10.13039/501100011033 and by ERDF "A way of making Europe" (EU).

**References**

[1] N. Asnafi, On stretch and shrink flanging of sheet aluminium by fluid forming, J. Mat. Proc. Tech. 96 (1999) 198–214. https://doi.org/10.1016/S0924-0136(99)00352-0

[2] H. Livatyali, A. Müderrisoğlu, M.A. Ahmetoğlu, N. Akgerman, G.L. Kinzel, T. Altan, Improvement of hem quality by optimizing flanging and pre-hemming operations using computer aided die design, J. Mater. Proc. Tech. 98 (2000) 41-52. https://doi.org/10.1016/S0924-0136(99)00304-0

[3] L. Chen, H. Chen, Q. Wang, Z. Li, Studies on wrinkling and control method in rubber forming using aluminium sheet shrink flanging process, Mater. Des. 65 (2015) 505-510. https://doi.org/10.1016/j.matdes.2014.09.057

[4] S. Kumar, M. Ahmed, S.K. Panthi, Effect of punch profile on deformation behaviour of AA5052 sheet in stretch flanging process, Archiv. Civ. Mech. Eng 20 (2020) 18. https://doi.org/10.1007/s43452-020-00016-2

[5] H. Zhang, Z. Zhang, H. Ren, J. Cao, J. Chen, Deformation mechanics and failure mode in stretch and shrink flanging by double-sided incremental forming, Int. J. Mech. Sci. 144 (2018) 216-222. https://doi.org/10.1016/j.ijmecsci.2018.06.002

[6] M. Borrego, D. Morales-Palma, A.J. Martínez-Donaire, G. Centeno, C. Vallellano, Analysis of formability in conventional hole flanging of AA7075-O sheets: punch edge radius effect and limitations of the FLC, Int. J. Mater. Form. 13 (2020) 303-316. https://doi.org/10.1007/s12289-019-01487-2

[7] M. Borrego, D. Morales-Palma, C. Vallellano, Analysis of Flangeability by Single-Stage SPIF and Press-Working in AA7075-O Sheet, *J. Manuf. Sci. Eng.* 143(1) (2020) 011005. https://doi.org/10.1115/1.4047997

[8] L. Belhassen, S. Koubaa, M. Wali, F. Dammak, Numerical prediction of springback and ductile damage in rubber-pad forming process of aluminum sheet metal, Int. J. Mech. Sci. 117 (2016) 218-226. https://doi.org/10.1016/j.ijmecsci.2016.08.015